The Astrophysical Journal, 621:167–175, 2005 March 1
© 2005. The American Astronomical Society. All rights reserved. Printed in U.S.A.

AN X-RAY VIEW OF WEAK-LINE RADIO GALAXIES/LINERs

Alexander S. Rinn, Rita M. Sambruna, and Mario Gliozzi
Department of Physics and Astronomy, George Mason University, MS 3F3, 4400 University Drive, Fairfax, VA 22030
Received 2004 July 6; accepted 2004 October 7

ABSTRACT

We present X-ray observations of nine weak-line radio galaxies (WLRGs), optically classified as confirmed or possible LINERs. The data were taken from the *Chandra*, *XMM-Newton*, and *BeppoSAX* archives. The *Chandra* images typically show complex X-ray morphologies, with hard (2–10 keV) point sources embedded in diffuse soft (0.3–2.0 keV) emission in all cases except those of 1246−41 (NGC 4696), in which only diffuse emission is detected on the scale of the cluster, and 0334−01 (3C 15), in which only a point source is detected. The nuclear X-ray spectra are well fitted at hard energies by an absorbed power law, with a wide range of photon indices, $\Gamma = 1.5$–2.7. Excess absorption over the Galactic value is detected in six of the nine sources, with column densities $N_{\rm H} \approx 10^{21}$–$10^{22}$ cm^{-2}. A thermal component is required at softer energies, in agreement with the results of the spatial analysis. We find that there is no correlation between the core X-ray luminosity and the radio core dominance parameter, suggesting that the bulk of the core X-ray emission is not beamed but rather is isotropic and thus likely related to the accretion flow. In an attempt to constrain the nature of the accretion flow, we calculate the ratios of bolometric to Eddington luminosities, $L_{\rm bol}/L_{\rm Edd}$, and the radiative efficiency η based on the Bondi accretion rates. We find that $L_{\rm bol}/L_{\rm Edd} \sim 10^{-4}$–$10^{-6}$ and $\eta \sim 10^{-2}$–10^{-6} for all the objects in our sample, suggesting radiatively inefficient accretion flows.

Subject headings: galaxies: active — galaxies: nuclei — X-rays: galaxies

1. INTRODUCTION

The recent discovery by the *Hubble Space Telescope* (*HST*) and ground-based observations that most nearby galaxies harbor supermassive black holes (Kormendy & Richstone 1995; Richstone et al. 1998), along with independent evidence that weak nuclear activity is very common in both spiral and elliptical galaxies (Heckman 1980; Sadler et al. 1989; Tadhunter et al. 1998), affirms the fundamental link between "normal" and active galaxies. According to the Palomar survey (Ho et al. 1997), over 40% of nearby galaxies ($z \approx 0$) contain low-power active galactic nuclei (AGNs), with typical bolometric luminosities lower than 10^{44} ergs s^{-1}. Most of these, based on their low-ionization spectra, are classified as LINERs, or transition objects. Since accreting supermassive black holes are widely held to be responsible for the nuclear activity in AGNs, one naturally wonders why such intense nuclear activity is limited to a minority of galaxies. A possible explanation is that obscuring material along the line of sight conceals the nuclear activity. Alternatively, there could be inefficient accretion onto the black hole due to either a low accretion rate (the AGN-starved scenario) or some kind of radiatively inefficient accretion flow (see, e.g., Quataert 2003). Weak AGNs, such as those hosted by nearby low-power radio galaxies in giant ellipticals, may represent the link between powerful AGNs and "normal" galaxies.

One class of objects that may represent this link are weak-line radio galaxies (WLRGs; Tadhunter et al. 1998), which are classified by [O III] λ5007 luminosities more than 10 times lower than those of the general population at similar redshifts. The weakness of the [O III] λ5007 emission line in WLRGs raises the possibility that these objects may be related to LINERs; indeed, there is evidence that WLRGs and LINERs are intimately related (Lewis et al. 2003). If all LINERs can be regarded as true AGNs, then they would constitute approximately 75% of all AGNs (Ho et al. 1997). Put in this light, WLRGs/LINERs could prove essential to understanding the link between "normal" and active galaxies.

X-rays provide us with a powerful tool by which we can achieve progress in our understanding of the nature of accretion in low-power AGNs because they originate in the innermost, hottest parts of the accretion flow. In addition, soft X-rays map the distribution of the circumnuclear gas around the nuclei, allowing us to quantify the fuel reservoir on the nucleus.

In § 2 we describe our sample of WLRGs/LINERs. In § 3 we describe the observations and data reduction. Section 4 contains the results of the spatial analysis based on *Chandra* observations (§ 4.1) and the results of the temporal and spectral analysis (§§ 4.2 and 4.3, respectively), both of which are based on *Chandra*, *XMM-Newton*, and *BeppoSAX* observations. In § 5 we discuss the obscuration and nature of accretion in WLRGs/LINERs, as well as some comparisons with the results of previous work. Finally, in § 6 we summarize our results. Throughout the paper we use a Friedmann cosmology with $H_0 = 75$ km s^{-1} Mpc^{-1} and $q_0 = 0.5$.

2. THE SAMPLE

Our sample consists of nine out of the 24 WLRGs that comprise the Lewis et al. (2003) sample. That sample was selected in order to investigate the relationship between WLRGs and LINERs. Our nine sources were selected based on two criteria: first, that Lewis et al. classified the source as a LINER or a possible LINER or that there were conflicting classifications; second, that there existed X-ray observations for the sources made by either *Chandra*, *XMM-Newton*, or *BeppoSAX*.

Table 1 lists some characteristics of the sources in our sample. It should be noted that all the sources have redshifts $z < 0.1$. The black hole masses were calculated using the relationship $M_{\rm BH} = 1.3 \times 10^8 (\sigma/200 \text{ km s}^{-1})^{4.58}$ (Ferrarese 2002; Merloni et al. 2003) and using velocity dispersions from the online catalog HyperLeda[1] unless otherwise specified in the table. These calculations were consistent with those found in the literature.

[1] Available at http://foehn.univ-lyon1.fr/hypercat/search.html.

TABLE 1
Object Sample

Object (1)	Alternate Name (2)	R.A. (J2000) (3)	Decl. (J2000) (4)	z (5)	N_H^{Gal} (10^{20} cm^{-2}) (6)	log M_{BH} (log $M_\odot$) (7)	FR (8)	LINER (9)
0034−01	3C 15	00 37 04.1	−01 09 08	0.007	2.9	8.81	I/II	C
0305+03	3C 78	03 08 26.2	+04 06 39	0.029	10.3	8.71	I	PL
0320−37	For A	03 22 41.7	−37 12 30	0.006	1.9	8.31	I	PL
0915−11	Hyd A	09 18 05.7	−12 05 44	0.054	4.9	8.97	I	L
1216+06	3C 270	12 16 23.2	+05 49 31	0.007	1.5	8.72	I	L
1246−41	NGC 4696	12 48 49.3	−41 18 40	0.010	8.1	8.65	I	L
1251−12	3C 278	12 54 36.1	−12 33 48	0.015	3.6	8.64	I	L
1333−33	IC 4296	13 36 39.0	−33 57 57	0.013	4.1	9.16	I/II	L
1637−77	PKS 1637−77	16 44 16.1	−77 15 48	0.043	8.7	8.68	II	L

Note.—Units of right ascension are hours, minutes, and seconds, and units of declination are degrees, arcminutes, and arcseconds. Col. (1): Object's IAU name. Col. (2): Object's common name. Cols. (3)–(4): Right ascension and declination from NED. Col. (5): Redshift from NED. Col. (6): Galactic equivalent hydrogen column density. Col. (7): Black hole masses calculated using the velocity dispersion–M_{BH} correlation (Ferrarese 2002), except for 0034−01 and 1637−77 from Bettoni et al. (2003) and 1216+06 from Ferrarese et al. (1996). Col. (8): Fanaroff & Riley (1974) radio classification from Tadhunter et al. (1998), except for 0034−01, which is from Leahy et al. (1997). Col. (9): Classification from Lewis et al. (2003): (L) LINER; (PL) possible LINER; (C) conflicting.

In addition, there is only one source that is classified as a Fanaroff-Riley type II galaxy (FR II galaxy; Fanaroff & Riley 1974) (1637−77); the rest of the sources are classified as either Fanaroff-Riley type I galaxies (FR I galaxies) or transition objects (FR I/II galaxies). Finally, we list how Lewis et al. (2003) classified the sources: six of the sources are confirmed LINERs, two are possible LINERs, and one is conflicting.

3. OBSERVATIONS AND DATA REDUCTION

Table 2 summarizes the X-ray observations of the sources comprising our sample. We used seven *Chandra* observations, four *XMM-Newton* observations, and one *BeppoSAX* observation.

3.1. *Chandra*

All the *Chandra* observations were made using the ACIS-S detector. Pileup was not a problem in any of the observations. The data reduction was performed with CIAO, version 2.3, and CALDB, version 2.18. The data were reprocessed with *acis_process_events* and screened to exclude periods of background flaring. In order to take into account the continuous degradation of the ACIS quantum efficiency due to molecular contamination of the optical blocking filters, we applied *acisabs* to the ancillary response function file.

The spectra were rebinned (with the exception of 1251−12) such that each spectral bin contained at least 20 counts in order to apply χ^2 minimization and were fitted using the XSPEC, version 11.2, software package (Arnaud 1996). Because of the very low number of counts, we did not rebin the spectrum of 1251−12, and instead of the χ^2 statistics, we used the C-statistics when fitting the spectrum. The quoted errors on the derived best-fit model parameters correspond to a 90% confidence level. The latest publicly available responses were used. The same procedure was applied to the *XMM-Newton* and *BeppoSAX* spectral analysis.

3.2. *XMM-Newton*

The *XMM-Newton* analysis was based on the EPIC pn data, since they have the highest signal-to-noise ratio among the

TABLE 2
Observation Log

Object (1)	Satellite (2)	Date (3)	Exposure (ks) (4)	r_{ext} (arcsec) (5)	Counts (6)
0034−01	*CXO*	2000 Nov 6	25.4	1.5	493 ± 22
0305+03	*SAX*	1997 Jan 7	19.4	240	672 ± 27
0320−37	*CXO*	2001 Apr 17	29.1	1.5	464 ± 22
0915−11	*CXO*	1999 Nov 2	17.8	1.5	400 ± 20
	XMM	2000 Dec 8	20.2	15.0	28810 ± 170
1216+06	*CXO*	2000 May 6	32.0	1.5	1738 ± 41
	XMM	2001 Dec 16	21.3	20.0	6454 ± 85
1246−41	*CXO*	2000 May 22	31.7	12.0	16719 ± 136
	XMM	2002 Jan 3	40.0	15.0	33055 ± 236
1251−12	*CXO*	2002 Jun 16	48.6	1.5	154 ± 12
1333−33	*CXO*	2001 Dec 15	24.3	1.5	1723 ± 42
1637−77	*XMM*	2002 Feb 23	3.5	15.0	1961 ± 45

Note.—Col. (1): Object's name. Col. (2): Satellite with which the object was observed: (*CXO*) *Chandra*; (*XMM*) *XMM-Newton*; (*SAX*) *BeppoSAX*. Col. (3): Date of observation. Col. (4): Effective exposure time. Col. (5): Radius of circular extraction region centered about the nucleus. Col. (6): Background-corrected number of counts in the extraction region; the energy range of the counts is dependent upon the detector used: ACIS-S is 0.5–8.0 keV, *XMM* is 0.3–10.0 keV, and *SAX* is 0.3–10.0 keV.

EPIC cameras. For 0915−11 and 1637−77 the EPIC pn operated in full-frame extended mode with a thin filter. For 1216+06 and 1246−41 the EPIC pn operated in full-frame mode with a thin filter. The recorded events were reprocessed and screened with the latest available release of the *XMM-Newton* Science Analysis Software (SAS ver. 5.4) to remove known hot pixels, and other data flagged as bad; only data with FLAG = 0 were used. We investigated the full-field light curves to detect periods of background flaring; any such events were screened. In 0915−11, 1216+06, and 1637−77, background data were extracted from a source-free circular region on the same chip containing the source. In 1246−41 background data were extracted in an annular region centered about the nuclear extraction region; this was done in an attempt to take into account the cluster in which this source lies. There are no signs of pileup in any of the sources.

3.3. *BeppoSAX*

BeppoSAX observed 0305+03 (3C 40) with the narrow field-instruments, LECS (0.1–4.5 keV) and MECS (1.3–10.0 keV), on 1997 January 7, with effective exposures of 8.7 and 19.4 ks, respectively. The LECS and MECS are both imaging instruments. The observations were performed with two active MECS units. Standard data reduction techniques were employed, following the prescription given by Fiore et al. (1999). LECS and MECS spectra and light curves were extracted from regions with radii of $8'$ and $4'$, respectively, in order to maximize the accumulated counts at both low and high energies. Background spectra were extracted from high Galactic latitude "blank" fields. The background-subtracted count rates are $(3.7 \pm 0.3) \times 10^{-2}$ counts s^{-1} for the LECS in the 0.1–4.5 keV band and $(3.5 \pm 0.1) \times 10^{-2}$ counts s^{-1} for the MECS in the 2–10 keV energy band.

4. RESULTS

4.1. *Spatial Analysis*

Chandra's subarcsecond spatial resolution provides us with the opportunity to disentangle the different X-ray components in a given source. In particular, the detection of a hard X-ray nuclear point source lends support to the claim that a source houses an AGN. Whatever the results of the spatial analysis are, they help one to better constrain and interpret the spectral data associated with the source.

For each of the objects in our sample observed by *Chandra* (except 1216+06, for which a more detailed spatial analysis is given in Gliozzi et al. 2003), Figure 1 shows the adaptively smoothed images in the energy band 0.3–10 keV with hard X-ray contours superposed (2–10 keV); also shown are the surface brightness profiles. The images were smoothed using *fadapt* from the FTOOLS software package. To produce the surface brightness profiles, we first used the source energy spectrum to derive the appropriate point-spread function (PSF) with ChaRT.[2] We then fit the ChaRT PSF in order to find an analytic description of it. Next we fit the total surface brightness profile with both the analytic PSF and either one or two β-models (e.g., Cavaliere & Fusco-Femiano 1976) in order to describe the extended emission. Finally, we used an *F*-test to assess the significance of the PSF by comparing the PSF plus β-model to a β-model alone.

The results of the spatial analysis are summarized in Table 3. All the objects, except 1246−41, required a PSF at high significance level. We found that only 0034−01 required no β-model; it was fitted well by the PSF plus the background. The object 0915−11 was fitted well by a PSF plus β-model out to $\approx 25''$. Past $\approx 25''$ the source appears to require another β-model, but we could not get good statistics on a second β-model, perhaps because the field of view was not large enough. We found that 1246−41 does not require a PSF, and while it too appears to require an additional β-model past $\approx 25''$, we could not get good statistics on a second β-model. For 1333−33 we were required to fix the value for the core radius in order to arrive at physically meaningful results; several different values were tried, with the quoted value yielding the best fit (also see Pellegrini et al. 2003).

4.2. *Timing Analysis*

We produced background-subtracted light curves for each of the objects in our sample. For 1216+06 we refer to the detailed study by Gliozzi et al. (2003). We chose to produce light curves based on *XMM-Newton* data when possible, but when only *Chandra* or *BeppoSAX* data were available, those data were used. According to a χ^2 test for constancy, we found there to be no statistically significant nuclear variability in any of the objects on the timescales probed by our observations, about a few hours. This is likely because of (1) the intrinsic weakness of the sources, which translates into a low count rate, especially for *Chandra* and *BeppoSAX* observations, and (2) the short exposures.

4.3. *Spectral Analysis*

Previous X-ray spectral studies of low-power radio galaxies suggest that at least two components are required to fit a spectrum: (1) a thermal component associated with the extended emission and (2) a power-law component associated with the unresolved nuclear point source (Worrall & Birkinshaw 1994). This is consistent with the results of our spatial analysis, in which four out of the six sources required a pointlike source in diffuse emission. With these considerations in mind we began our spectral modeling with a power law, which dominates at hard energies, and a soft component modeled as emission from a collisionally ionized plasma (*apec* in XSPEC; Smith et al. 2001). All the spectral models also assume a column density fixed to the Galactic level appropriate to the source (Dickey & Lockman 1990). Additional components, such as intrinsic absorption, covering fraction, or additional thermal components, were added to the model when the data required them.

The results of the spectral analysis are summarized in Table 4. When a source was observed with both *XMM-Newton* and *Chandra* we quote the spectral model derived from the *XMM-Newton* data, since it was more statistically sound. Seven out of the nine objects require a power law with Γ between $\sim$1.5 and $\sim$2.7, with the average value being $\sim$1.9. The extremely flat value of Γ for 1251−12 might be related to the poor photon statistics. Six out of the nine objects required at least one thermal component. The temperatures show a bimodal distribution around 0.6 and >1.5 keV, which probably reflects the different environments, poor and rich clusters, respectively. Five out of the nine objects required intrinsic absorption with values ranging from $\sim 10^{21}$ to $\sim 10^{23}$ cm^{-2}, with the average value being $\sim 4 \times 10^{23}$. We tried to add a Fe Kα line at 6.4 keV, but this was not statistically required for any of the objects except 1216+06 (see Sambruna et al. 2003).

The spectral results are in good agreement with the findings of the spatial analysis. The surface brightness profile of 0034−01 was found to not require a β-model, indicating that little to

[2] See http://cxc.harvard.edu/soft/ChaRT/cgi-bin/www-saosac.cgi.

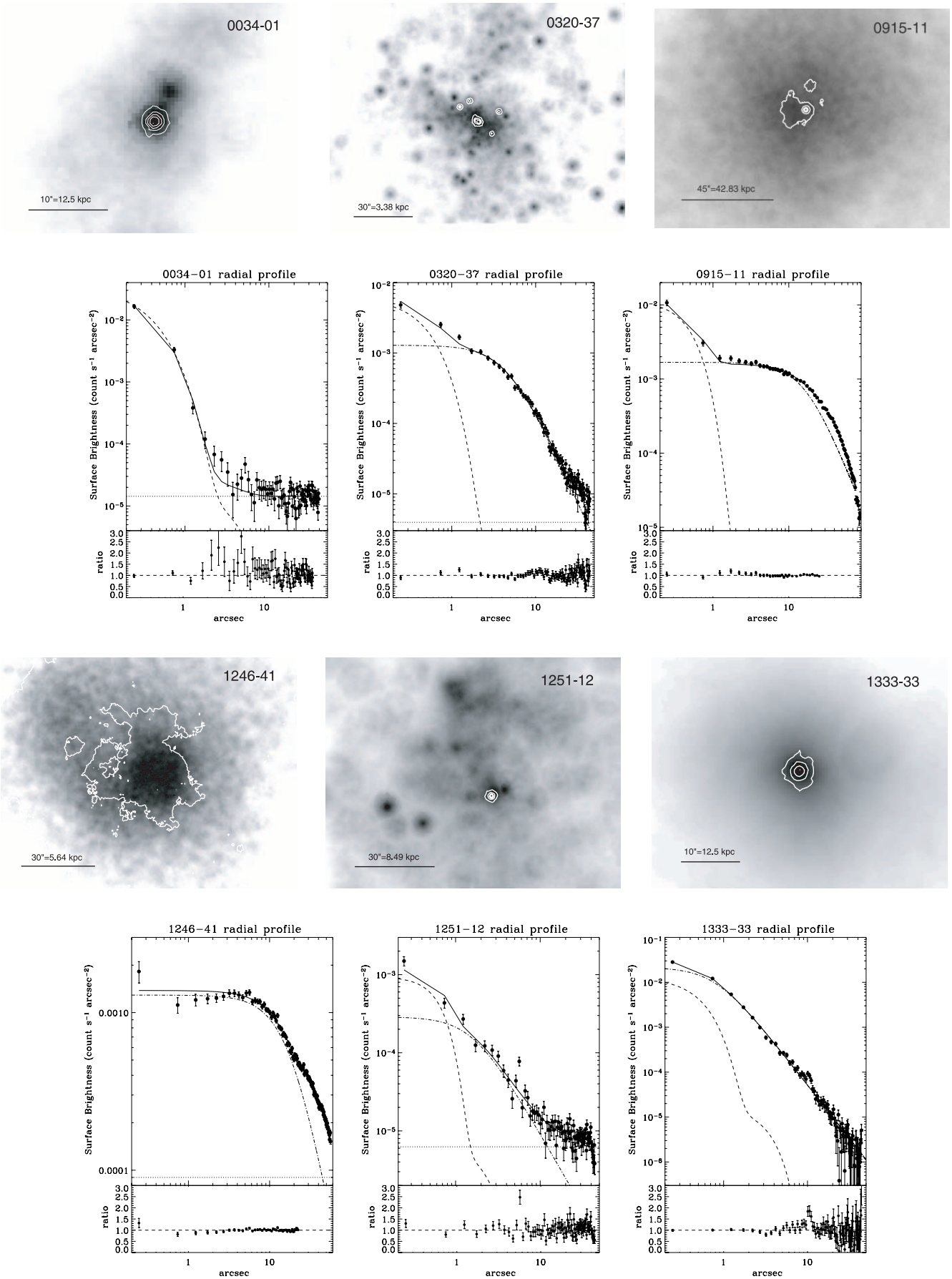


FIG. 1.—*Rows 1 and 3, from the top*: Adaptively smoothed *Chandra* images in the 0.3–10 keV range, with hard contours (2–10 keV) overlaid. *Rows 2 and 4*: Corresponding surface brightness profiles with best-fit (*solid line*), PSF (*dashed line*), and β-model (*dot-dashed line*) overlaid.

TABLE 3
RESULTS OF SPATIAL ANALYSIS

Object (1)	R_c (arcsec) (2)	β (3)	N_β (10^{-4}) (4)	P_{PSF} (5)
0034−01	...	...	...	>99.9
0320−37	4.6 ± 0.3	0.61 ± 0.06	12.59 ± 0.008	>99.9
0915−11	15.9 ± 1.6	0.47 ± 0.10	15.85 ± 0.316	>99.9
1246−41	18.8 ± 2.0	0.64 ± 0.20	12.59 ± 0.199	16.6
1251−12	1.8 ± 0.5	0.49 ± 0.11	2.512 ± 0.631	>99.9
1333−33	0.8_{fixed}	0.56 ± 0.01	199.5 ± 7.943	>99.9

NOTE.—Col. (1): Object's name. Col. (2): Core radius. Col. (3): β-value. Col. (4): Normalization on the β-model. Col. (5): Probability that a PSF is required according to an *F*-test.

no extended emission is present; indeed, we see that no thermal component is required to fit the object's spectrum. We also found that the surface brightness profile of 1246−41 did not require a PSF, indicating a heavily absorbed and/or very weak point source; this too conforms to the spectral results, in that no power law was required to fit the object's spectrum.

5. DISCUSSION

This paper seeks to shed light on the role of WLRGs/LINERs in the context of uncovering the relationship between "normal" galaxies and powerful AGNs. The results of the X-ray analysis allow us to address several important questions toward this end: (1) What is the role of obscuration in WLRGs/LINERs? (2) What is the nature of accretion in such objects? (3) How do the X-ray properties of WLRGs/LINERs compare to those of other classes of radio galaxies?

5.1. *The Role of Obscuration*

According to the unified model of AGNs (e.g., Urry & Padovani 1995), the central regions of AGNs appear to contain a molecular torus that prevents the penetration of radiation from the nucleus along certain lines of sight. This can cause intrinsically similar AGNs to look remarkably different from different viewing angles. Recently, however, the presence of an obscuring torus in low-power radio galaxies, specifically FR I galaxies, has been called into question (Chiaberge et al. 1999, hereafter C99; Capetti et al. 2002, hereafter C02), based on *HST* observations of the Third Cambridge (3C) and Second Bologna (B2) catalogs. Since our sample is composed of low-power radio galaxies, and because our analysis is focused on the X-rays, we are in a position to contribute to this debate. X-rays, because of their high penetrating power, are the ideal means by which the presence of an obscuring torus can be investigated.

The results of our spectral analysis show that four of the nine objects in our sample require an absorption component on the order of 10^{22} cm^{-2}, which qualifies as significant absorption. Out of those four objects, three are confirmed LINERs, while one is classified as conflicting. In addition to these four objects there are two others that, while not heavily absorbed, require an absorption component on the order of 10^{21} cm^{-2}; one of these additional objects is a confirmed LINER, the other is a possible LINER. Thus, six of nine objects in our sample show signs of absorption, which suggests that some low-power radio galaxies may indeed house obscuring tori. Moreover, all six of these absorbed objects are classified as FR I galaxies or transition objects (FR I/II galaxies), which is in contrast to the hypothesis that low-power radio galaxies, specifically FR I galaxies, lack a molecular torus (C99; C02). The apparently surprising result that the only FR II galaxy in our sample (1637−77) that is not absorbed may be explained if the object can be classified as a low-excitation galaxy (LEG); Chiaberge et al. (2002) explain that, while LEGs may be classified morphologically as FR II galaxies, their radio to optical nuclear properties are indistinguishable from FR I galaxies. The [O II]/[O III] ratio for 1637−77 places it right on the border of the LEG classification, but if 1637−77 can be classified as an LEG, we should expect it to be unabsorbed.

In order to address the apparent discrepancy between the optical/UV and the X-ray absorption properties, one must keep

TABLE 4
RESULTS OF SPECTRAL ANALYSIS

Object (1)	Model[a] (2)	kT (keV) (3)	Abundance (4)	N_H^{add} (10^{22} cm^{-2}) (5)	CF (6)	EW (eV) (7)	Γ (8)	χ^2_{red}/dof (9)
0034−01	I	...	...	$8.8^{+3.5}_{-2.4}$	0.86 ± 0.06	<170	$1.58^{+0.29}_{-0.32}$	0.73/19
0305+03	IV	...	...	...	...	<1900	$2.74^{+0.26}_{-0.25}$	0.98/31
0320−37	II	0.6 ± 0.1	0.2_{fixed}	$0.3^{+1.3}_{-0.3}$	...	...	$1.78^{+1.21}_{-0.40}$	0.90/15
0915−11	VI	$1.8^{+0.34}_{-0.56}$	$0.2^{+0.05}_{-0.09}$	$6.0^{+6.3}_{-2.4}$	...	<51.3	$2.14^{+1.26}_{-0.58}$	1.03/548
	...	$4.3^{+2.30}_{-1.01}$	$1.2^{+0.00}_{-0.64}$	...	...	...	...	...
1216+06	III	$0.7^{+0.01}_{-0.02}$	1.0_{fixed}	$5.1^{+1.1}_{-1.2}$	$0.81^{+0.06}_{-0.09}$	230^{+166}_{-134}[b]	$1.46^{+0.17}_{-0.31}$	1.12/359
1246−41	V	0.7 ± 0.01	$1.2^{+0.00}_{-0.07}$	0.1 ± 0.01[c]	...	<374	...	1.23/483
	...	1.5 ± 0.02	$1.2^{+0.00}_{-0.02}$	...	...	...	...	...
1251−12	VII	0.6 ± 0.1	$1.2^{+0.00}_{-0.93}$	...	...	...	$-0.07^{+0.58}_{-0.69}$	334/435[d]
1333−33	II	0.6 ± 0.3	1.0_{fixed}	$1.1^{+0.6}_{-0.5}$	...	...	$1.52^{+0.42}_{-0.37}$	1.22/66
1637−77	IV	...	...	...	...	<375	1.90 ± 0.06	0.76/88

NOTE.—Col. (1): Object's name. Col. (2): Spectral model (see footnote a). Col. (3): Plasma temperature. Col. (4): Metal abundances (solar =1.0). Col. (5): Absorption column density at the redshift of the source. Col. (6): Covering fraction. Col. (7): Equivalent width at $E_{line} = 6.4$ keV, with the physical width of the Gaussian model fixed at $\sigma = 0.01$ keV (see note for 1216+06). Col. (8): Photon index. Col. (9): χ^2_{red} and degrees of freedom.

[a] I = wabs[zpcfabs(powerlaw)]; II = wabs[apec + zwabs(powerlaw)]; III = wabs[apec + zpcfabs(powerlaw)]; IV = wabs(powerlaw); V = wabs(apec + apec); VI = wabs[apec + apec + wabs(powerlaw)]; VII = wabs(apec + powerlaw).

[b] More precise values of E_{line} and σ were able to be fitted for this object: $E_{line} = 6.99^{+0.08}_{-0.09}$ keV and $\sigma = 0.03^{+0.15}_{-0.03}$ keV.

[c] This is not an additional absorption component; such a component did not help the fit. This is the number to which the galactic absorption rose when we let it free.

[d] Because of the very low number of counts, we used the *C*-statistics to fit this model. Col. (9) therefore gives the *C*-statistics and the number of spectral bins.

in mind that the inner regions of the accretion flow ($\sim$10–50 R_G), where most of the radiation is supposed to originate, are inaccessible to any observatory. Although the angular resolution of *HST* ($\sim$0.″1) is much better than those of *Chandra* ($\sim$1.″0) and *XMM-Newton* ($\sim$10″), the region probed by *HST* is not closer to the black hole than those probed by the X-ray satellites. Indeed, assuming a typical black hole mass of $5 \times 10^8\ M_\odot$ at a distance of 40 Mpc (corresponding to $z \sim 0.01$), the inner 50 R_G subtends a region of angular size $\sim 10^{-4}$ arcsec, which is 3 orders of magnitude smaller than the spatial resolution of *HST*. This indicates that the unresolved X-ray and optical sources simply reflect the PSF of the respective instrument rather than the physical size of the emitting regions.

In light of these considerations, it is entirely possible that the X-ray emission is produced in a region closer to the black hole than that of the optical/UV-emitting region. Indeed, theoretical arguments predict that the X-ray–emitting region is closer to the black hole in both accretion and jet models. This hypothesis is supported by the difference in absorption properties found in the optical/UV and the X-rays, if it is assumed that two distinct media are responsible for the absorption (Weingarter & Murray 2002; Sambruna et al. 2003; Lewis et al. 2003). In this theory, the optical/UV absorber is a dusty medium lying farther away from the nucleus than the X-ray absorber, which is a neutral or ionized gas largely free of dust. Further support for the hypothesis that the X-rays are produced in a region interior to the optical/UV-emitting region comes from the recent work of Donato et al. (2004). Those authors find that a substantial fraction of the compact cores detected in the optical (C99) do not have an unresolved X-ray counterpart, which suggests a different origin and/or nature for optical/UV and X-ray radiation. In addition, Donato et al. show that neither X-ray obscuration nor the detection of unresolved X-ray cores is related to the presence of dust lanes, which are responsible for the optical absorption. Finally, we note that there is no discrepancy between this paper and Donato et al. (2004) concerning obscuration; in that paper all the FR I galaxies except the LINER 1216+06 (NGC 4261) show negligible absorption ($N_{\rm H} < 10^{21}$ cm^{-2}). This suggests that the absorption mechanisms in WLRGs/LINERs may be different from those in other low-luminosity radio galaxies.

5.2. *The Nature of Accretion*

The origin of X-rays in radio galaxies is a topic of considerable debate. Specifically, the question is: Do X-rays have their origin in the process of accretion or at the unresolved base of the jet? The correlation between the radio and X-ray core luminosities in low- and high-luminosity radio galaxies (e.g., Fabbiano et al. 1984; Canosa et al. 1999; Worrall & Birkinshaw 1994; Hardcastle et al. 1998) has often been used as an argument in favor of a common origin at the base of the jet. However, this correlation has recently been shown by Merloni et al. (2003) to derive from a more general correlation involving both the X-ray luminosity and the black hole mass—the so-called fundamental plane—in which the radio is related to the jet, and the X-rays are related to inefficient accretion onto the black hole.

This idea is supported by the detailed study of 1216+06 (NGC 4261) by Gliozzi et al. (2003); their argument is summarized by three main points: (1) they found there to be a high Bondi accretion rate along with a low AGN luminosity, suggesting the presence of a radiatively inefficient accretion flow; (2) they observed an Fe line at $\approx$7 keV of nuclear origin; and (3) they studied the temporal and spectral variability and combined this with independent information on jet energetics, which led them to conclude that the bulk of the X-ray emission originates from a radiatively inefficient accretion flow, with negligible jet contribution. Based on the similarity between 1216+06 and the other objects in our sample, we explored the possibility that the X-rays for all the objects in our sample are related to accretion and not the base of the jet.

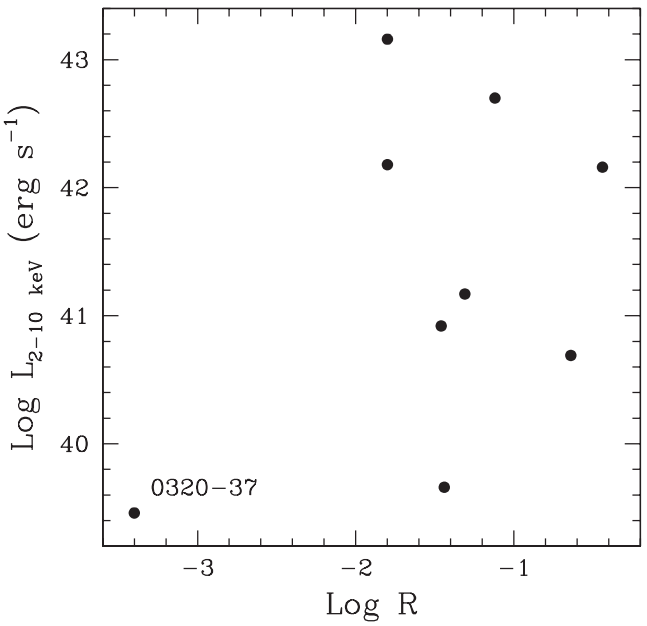


FIG. 2.—Radio core dominance R vs. the 2–10 keV intrinsic luminosity. The parameter R is defined as a ratio of the core-to-lobes 5 GHz luminosities from Morganti et al. (1993). No correlation between the core X-ray luminosity and the radio core dominance is apparent.

One way to explore the origin of nuclear emission is via the correlation (or lack thereof) with the radio core dominance ($R = L_{\rm core}/L_{\rm lobe}$); this has been done in the optical by Kharb & Shastri (2004). By demonstrating a strong correlation between optical pointlike emission and radio core dominance, Kharb & Shastri found the optical emission to be strongly beamed and thus produced by the jet, confirming the results of C99. We adopted this approach for our X-ray sample (see Fig. 2 and Table 5) but found there to be no correlation between the core X-ray emission and the radio core dominance, indicating that the emission is not beamed but rather is isotropic and thus likely to be related to accretion. On the other hand, there is some indication that in non-LINER FR I galaxies at least a fraction of the X-ray emission is beamed and thus related to the base of the jet (Donato et al. 2004).

Many of the objects in our sample require a power-law component for their spectral fit, but the power-law components (ranging from $\Gamma \sim 1.5$ to $\sim$2.1, excluding the *BeppoSAX* observation with $\Gamma \sim 2.7$) can be a good representation for both jet-dominated and accretion-dominated emission. The lack of a strong Fe Kα line suggests the lack of a standard accretion disk; however, both the radiatively inefficient accretion and the jet scenario can account for this result. While temporal analysis can yield insights into the nature of accretion, our results yield no such clues.

More insightful information comes from the calculations of the bolometric and Eddington luminosities. We used estimates of the black hole masses based on stellar velocity dispersions to calculate $L_{\rm Edd}$ and the relationship $0.1 L_{\rm bol} = L_{\rm X}$ in order to calculate $L_{\rm bol}$. For Seyfert-like objects, which are thought to have a standard thin disk, the ratio of $L_{\rm bol}$ to $L_{\rm Edd}$ is $\sim$10%–20%; an Eddington ratio much less than 10% could signify

TABLE 5
LUMINOSITIES

Object (1)	$L_{5\ \mathrm{GHz}}$ (ergs s^{-1}) (2)	$L_{12\ \mu\mathrm{m}}$ (ergs s^{-1}) (3)	$L_{[\mathrm{O\ III}]}$ (ergs s^{-1}) (4)	$L_{2-10\ \mathrm{keV}}$ (ergs s^{-1}) (5)	R (6)
0034−01	41.84	...	40.41	40.69	−0.64
0305+03	41.84	<45.36	39.12	42.16[a]	−0.44
0320−37	41.24	42.94	<38.65	39.46	−3.40
0915−11.....	42.58	<46.63	40.27	42.18	−1.80
	...	...	...	43.16[b]	...
1216+06	40.67	42.63	<41.06	40.92[b]	−1.46
1246−41	...	...	<38.17	<40.01[b]	...
1251−12.....	40.70	<46.07	<38.70	39.66	−1.44
1333−33	40.99	<44.38	<38.87	41.17	−1.31
1637−77	41.63	...	40.37	42.70[b]	−1.12

NOTE.—Values in cols. (2)–(5) are $\log(\nu L_\nu)$. References are as stated below except for 0320−37, 1216+06, and 1333−33, for which the values in cols. (2)–(4) and col. (6) come from Sambruna et al. (1999). Col. (2): 5 GHz lobe luminosity ($L_{\mathrm{tot}} - L_{\mathrm{core}}$) from Morganti et al. (1993). Col. (3): 12 μm luminosity from Golombek et al. (1988). Col. (4): [O III] λ5007 line luminosity from Tadhunter et al. (1998). Col. (5): 2–10 keV intrinsic luminosity, in which the default instrument is *Chandra*. Col. (6): *R*-value from Morganti et al. (1993), defined as the ratio of the core radio luminosity to the lobe radio luminosity at 5 GHz.

[a] Refers to *BeppoSAX*.

[b] Refers to *XMM-Newton*.

TABLE 6
ACCRETION PROPERTIES

Object (1)	$L_{\mathrm{bol}}/L_{\mathrm{Edd}}$ (10^{-6}) (2)	$\dot{M}_{\mathrm{Bon}}$ ($M_\odot$ yr^{-1}) (3)	η (10^{-5}) (4)
0034−01	6.020	...	...
0305+03	219.5	...	...
0320−37	1.126	0.05	1.106
0915−11.....	132.2	0.03	1017
0915−11[a]	1234	0.03	9490
1216+06	19.20	0.04	47.28
1246−41	1.825	0.07	2.485
1251−12.....	0.853	0.05	1.633
1333−33	8.154	6.41	0.407
1637−77	834.3	...	...

NOTE.—Col. (1): Object's name. Col. (2): Ratio of the bolometric luminosity to the Eddington luminosity. Col. (3): Bondi accretion rate. Col. (4): Radiative efficiency.

[a] Refers to values based on $L_{2-10\ \mathrm{keV}}$ from *XMM-Newton* observation.

inefficient accretion. Some accretion properties are listed in Table 6. In our sample we find that the majority of sources have values of $L_{\mathrm{bol}}/L_{\mathrm{Edd}}$ between 10^{-4} and 10^{-7}. Even the *XMM-Newton* observation of 0915−11, with its high X-ray luminosity, has $L_{\mathrm{bol}}/L_{\mathrm{Edd}} \sim 10^{-3}$. This is a model-independent indication of radiatively inefficient accretion flow. Using the results of our spatial analysis, specifically the gas density profile obtained by the deprojection of the surface brightness profile, we calculated $\dot{M}_{\mathrm{Bon}}$, which serves as a rough estimate of accretion onto the black hole. With $\dot{M}_{\mathrm{Bon}}$ and L_{bol} we can use the formula $L_{\mathrm{bol}} = \eta \dot{M}_{\mathrm{Bon}} c^2$ to make an estimate of the radiative efficiency of accretion η. We find values on the order of 10^{-5}–10^{-6}, except for the object 0915−11, which, using the *Chandra* observation, yields $\eta = 0.01$ and, using the *XMM-Newton* observation, yields $\eta = 0.09$. Those objects with $\eta \ll 0.1$ are very likely to have inefficient accretion, but even 0915−11, based on the *Chandra* observation, is a candidate. However, the *XMM-Newton* observation makes the accretion scenario for 0915−11 ambiguous.

5.3. *Comparison with Previous Results*

As mentioned above, Donato et al. (2004) have analyzed a larger sample of FR I galaxies from the B2 and 3C catalogues. Those authors found there to be no absorption of X-rays in FR I galaxies, except in the LINER 1216+06 (NGC 4261), which is consistent with our results. While Donato et al. found that the majority of the X-rays in classical FR I galaxies are related to inefficient accretion onto the black hole, their analysis suggests that at least a fraction of the X-rays are beamed and thus potentially related to the base of the jet. This lends further support to the idea that WLRGs/LINERs form a distinct group from classical FR I galaxies.

A more general X-ray analysis of radio-loud AGNs was made by Sambruna et al. (1999) using *ASCA*. In that paper the authors found there to be correlations for the [O III] λ5007, the 5 GHz lobe, and the 12 μm luminosities to the 2–10 keV intrinsic X-ray luminosity. Those correlations demonstrated a slight lobe radio excess in WLRGs. We have updated the plots of Sambruna et al. to include those WLRGs that were not in that paper and have introduced a plot of the 5 GHz core luminosity and the 2–10 keV intrinsic X-ray luminosity (see Table 5 and Fig. 3). These updated plots show that the WLRGs do indeed demonstrate a lobe radio excess; moreover, they form a distinct class as compared to the other subclasses of radio-loud AGNs. To quantify the degree of linear correlation between the 2–10 keV intrinsic luminosity and the 5 GHz lobe radio power for the WLRGs (and the other correlations that follow), we calculated the linear correlation coefficient r and computed the chance probability $P_c(r; N)$ that a random sample of N uncorrelated pairs of measurements would yield a linear correlation coefficient equal to or greater than $|r|$. We also calculated the Spearman and Kendall parameters, which confirm the $P_c(r; N)$ results. We found the probability of correlation between L_{lobe} and $L_{2-10\ \mathrm{keV}}$ for the WLRGs to be ≈98%, with a least-squares fit yielding the relationship $\log L_{\mathrm{lobe}} = 0.46 \log L_{2-10\ \mathrm{keV}} + 22.6$ (0.46 ± 0.1, 22.6 ± 5), represented by the dotted line in Figure 3. The remaining subclasses of AGNs formed a distinct group of their own with a probability of correlation of more than 99.9%; however, the least-squares fit of this group yielded a significantly different relationship: $\log L_{\mathrm{lobe}} = 0.84 \log L_{2-10\ \mathrm{keV}} + 5.26$ (0.84 ± 0.1, 5.26 ± 6), represented by the dashed line in Figure 3. This lobe excess in the WLRGs raises the possibility that there once was much more intense jet activity in these objects than is shown today.

The plot of the core radio power versus the intrinsic 2–10 keV luminosity shows that the WLRGs follow the correlation of the other subclasses of radio-loud AGNs. The probability of correlation is more than 99.9%, and a least-squares fit yields the relationship $\log L_{\mathrm{core}} = 0.51 \log L_{2-10\ \mathrm{keV}} + 18.56$ (0.51 ± 0.08, 18.56 ± 3.3).

The plot of the mid-IR (MIR) luminosity versus the intrinsic 2–10 keV luminosity suggests that there may also be an MIR excess. However, the MIR data for WLRGs are largely upper limits, so this suggestion should be taken with caution; in addition, because there were so many upper limits, we were not able to better constrain the correlation found by Sambruna et al. (1999); thus, Figure 3 plots that previously found relationship $L_{12\mu\mathrm{m}} = 0.83 \log L_{2-10\ \mathrm{keV}} + 8.28$. Finally, we found the probability of correlation between $L_{[\mathrm{O\ III}]}$ and $L_{2-10\ \mathrm{keV}}$ to be more than 99%, with a least-squares fit yielding the relationship

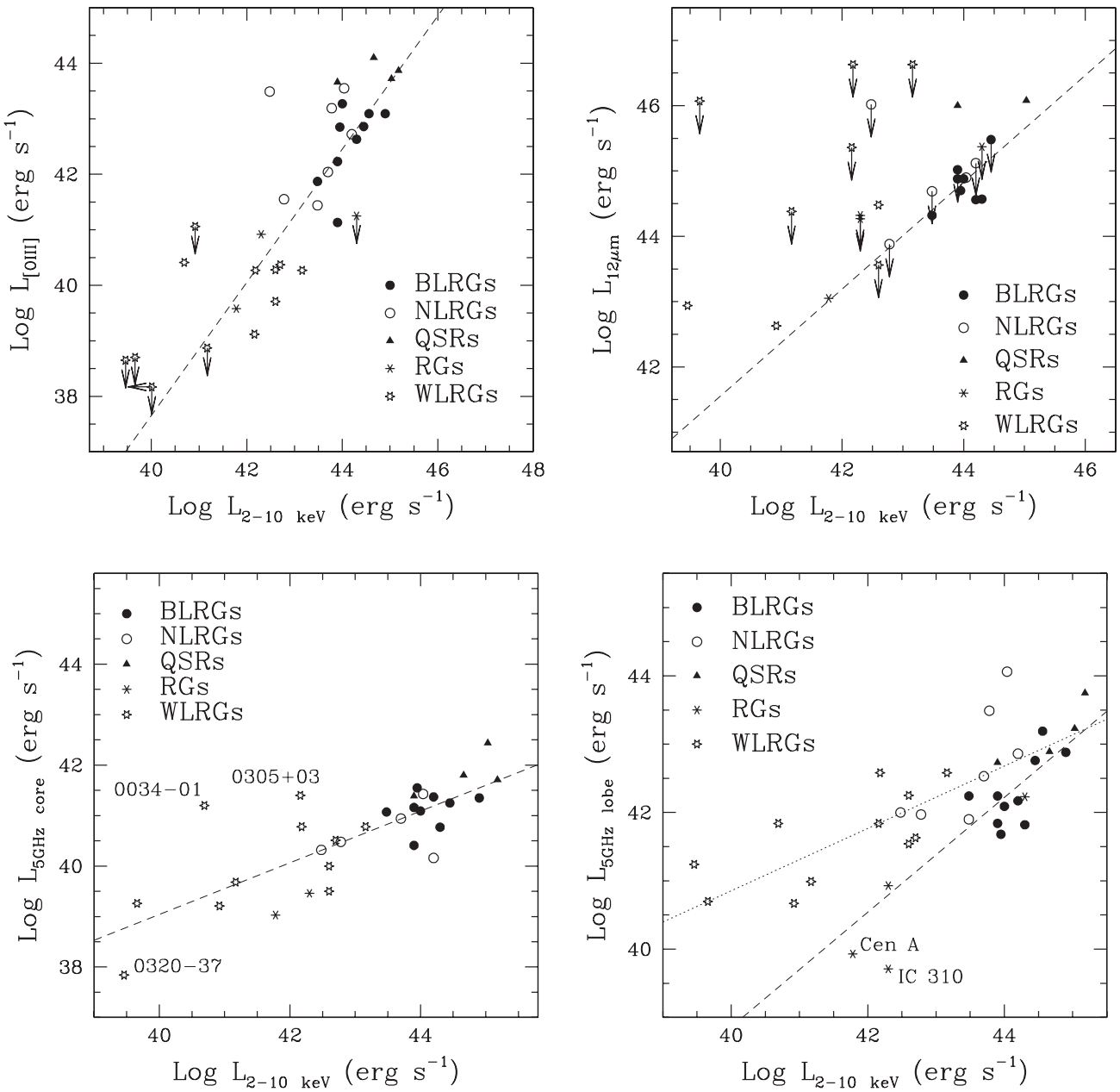


FIG. 3.—*Top left*: Correlation between the luminosity of the [O III] λ5007 emission line and the intrinsic 2–10 keV luminosity for various subclasses of radio-loud AGNs. Excluding the upper limits, a least-squares fit yields the relationship $\log L_{[\mathrm{O\ III}]} = 1.2 \log L_{2-10\ \mathrm{keV}} - 10.33$. *Top right*: Correlation between the MIR emission at 12 μm and the intrinsic 2–10 keV luminosity. Excluding the upper limits, the correlation is consistent with Sambruna et al. (1999). *Bottom left*: Core radio power at 5 GHz and the intrinsic 2–10 keV luminosity; a least-squares fit yields the relationship $\log L_{\mathrm{core}} = 0.51 \log L_{2-10\ \mathrm{keV}} + 18.56$. *Bottom right*: Correlation between the lobe radio power at 5 GHz and the intrinsic 2–10 keV luminosity. A least-squares fit of the broad-line radio galaxies (BLRGs), narrow-line radio galaxies (NLRGs), quasars (QSRs), and radio galaxies (RGs) yields the relationship $\log L_{\mathrm{lobe}} = 0.84 \log L_{2-10\ \mathrm{keV}} + 5.26$ (*dashed line*). However, the WLRGs formed a distinct group; a least-squares fit yields the relationship $\log L_{\mathrm{lobe}} = 0.46 \log L_{2-10\ \mathrm{keV}} + 22.6$ (*dotted line*).

$\log L_{[\mathrm{O\ III}]} = 1.2 \log L_{2-10\ \mathrm{keV}} - 10.33$ (1.2 ± 0.2, -10.33 ± 7), which is consistent within the errors with Sambruna et al. (1999). We notice that the WLRGs tend to have a slight [O III] deficiency; however, because of the small number of data points, we could not get good statistics for a least-squares fit of the WLRGs as a distinct class.

6. SUMMARY

This paper shows the results of an X-ray analysis of nine WLRGs/LINERs; the main findings are summarized as follows:

1. We found that six out of the nine objects in our sample are absorbed in X-rays. Four of these six objects are absorbed on the order of 10^{22} cm^{-2}, which qualifies as significant absorption. The other two objects show slightly lower values of absorption (10^{21} cm^{-2}). These results, combined with those of a larger sample of non-LINER FR I galaxies, for which there is a systematic lack of absorption, suggest that WLRGs/LINERs form a distinct class from other low-power radio galaxies.

2. The X-rays in this sample of WLRGs/LINERs appear to be related to accretion. The object 1216+06 has been carefully studied by Gliozzi et al. (2003), and the X-rays of that object are found to be related to accretion. We found that the rest of the objects in our sample behave like 1216+06, and while we cannot rule out that a fraction of the X-rays come from the base of the jet, we performed a model-independent test and found that

the X-rays in this sample do not appear to be beamed. On the other hand, the recent analysis of a sample of classical FR I galaxies reveals that, while the majority of the X-rays are related to inefficient accretion onto the black hole, a fraction of the X-rays may be beamed and thus likely related to the base of the jet. This lends further support to the idea that WLRGs/LINERs form a distinct class from other low-power radio galaxies.

3. Assuming that all the X-ray emission is related to accretion, our tests concerning the nature of accretion are in favor of it being radiatively inefficient. But even if some of the X-rays do stem from the base of the jet, the argument for radiatively inefficient accretion is only strengthened: the fraction of X-rays related to accretion would be even lower than we assumed them to be, which in turn would yield even lower efficiency.

Our results are based on a small sample of WLRGs/LINERs. These results should be confirmed by an analysis of a larger sample, which we plan to undertake in a future paper.

We gratefully acknowledge the financial support provided by Smithsonian grant GO3-4123A (A. S. R.) and NASA Long-Term Space Astrophysics (LTSA) grant NAG5-10708 (R. M. S., M. G.). R. M. S. gratefully acknowledges support from an NSF CAREER award and from the Clare Boothe Luce Program of the Henry Luce Foundation.

REFERENCES

Arnaud, K. 1996, in ASP Conf. Ser. 101, Astronomical Data Analysis Software and Systems V, ed. G. Jacoby & J. Barnes (San Francisco: ASP), 17
Bettoni, D., Falomo, R., Fasano, G., & Govoni, F. 2003, A&A, 399, 869
Canosa, C. M., Worrall, D. M., Hardcastle, M. J., & Birkinshaw, M. 1999, MNRAS, 310, 30
Capetti, A., Celotti, A., Chiaberge, M., de Ruiter, H. R., Fanti, R., Morganti, R., & Parma, P. 2002, A&A, 383, 104 (C02)
Cavaliere, A., & Fusco-Femiano, R. 1976, A&A, 49, 137
Chiaberge, M., Capetti, A., & Celotti, A. 1999, A&A, 349, 77 (C99)
———. 2002, A&A, 394, 791
Dickey, J. M., & Lockman, F. J. 1990, ARA&A, 28, 215
Donato, D., Sambruna, R. M., & Gliozzi, M. 2004, ApJ, 617, 915
Fabbiano, G., Miller, L., Trinchieri, G., Longair, M., & Elvis, M. 1984, ApJ, 277, 115
Fanaroff, B. L., & Riley, J. M. 1974, MNRAS, 167, 31P
Ferrarese, L. 2002, in Current High-Energy Emission around Black Holes, ed. C.-H. Lee & H.-Y. Chang (Singapore: World Scientific), 3
Ferrarese, L., Ford, H. C., & Jaffe, W. 1996, ApJ, 470, 444
Fiore, F., Guainazzi, M., & Grandi, P. 1999, Handbook for *BeppoSAX* NFI Spectral Analysis (Rome: *BeppoSAX* Science Data Center), ftp://www.sdc.asi.it/pub/sax/docs/saxabc_v1.2.ps.gz
Gliozzi, M., Sambruna, R. M., & Brandt, W. N. 2003, A&A, 408, 949
Golombek, D., Miley, G. K., & Neugebauer, G. 1988, AJ, 95, 26
Hardcastle, M. J., Worrall, D. M., & Birkinshaw, M. 1998, MNRAS, 296, 1098
Heckman, T. M. 1980, A&A, 87, 152
Ho, L. C., Filippenko, A. V., & Sargent, W. L. W. 1997, ApJ, 487, 568
Kharb, P., & Shastri, P. 2004, A&A, 425, 825
Kormendy, J., & Richstone, D. 1995, ARA&A, 33, 581
Leahy, J. P., Black, A. R. S., Dennett-Thorpe, J., Hardcastle, M. J., Komissarov, S., Perley, R. A., Riley, J. M., & Scheuer, P. A. G. 1997, MNRAS, 291, 20
Lewis, K. T., Eracleous, M., & Sambruna, R. M. 2003, ApJ, 593, 115
Merloni, A., Heinz, S., & di Matteo, T. 2003, MNRAS, 345, 1057
Morganti, R., Killeen, N. E. B., & Tadhunter, C. N. 1993, MNRAS, 263, 1023
Pellegrini, S., Venturi, T., Comastri, A., Fabbiano, G., Fiore, F., Vignali, C., Morganti, R., & Trinchieri, G. 2003, ApJ, 585, 677
Quataert, E. 2003, Astron. Nachr. Suppl., 324, 435
Richstone, D., et al. 1998, Nature, 395, A14
Sadler, E. M., Jenkins, C. R., & Kotanyi, C. G. 1989, MNRAS, 240, 591
Sambruna, R. M., Eracleous, M., & Mushotzky, R. 1999, ApJ, 526, 60
Sambruna, R. M., Gliozzi, M., Eracleous, M., Brandt, W. N., & Mushotzky, R. 2003, ApJ, 586, L37
Smith, R. K., Brickhouse, N. S., Liedahl, D. A., & Raymond, J. C. 2001, ApJ, 556, L91
Tadhunter, C. N., Morganti, R., Robinson, A., Dickson, R., Villar-Martin, M., & Fosbury, R. A. E. 1998, MNRAS, 298, 1035
Urry, M. C., & Padovani, P. 1995, PASP, 107, 803
Weingarter, J. C., & Murray, N. 2002, ApJ, 580, 88
Worrall, D. M., & Birkinshaw, M. 1994, ApJ, 427, 134